Quaternary Science Reviews 255 (2021) 106825

Contents lists available at ScienceDirect

Quaternary Science Reviews

journal homepage: www.elsevier.com/locate/quascirev

Middle Holocene Indian summer monsoon variability and its impact on cultural changes in the Indian subcontinent

Varsha Rawat [a], Suman Rawat [a, *], Priyeshu Srivastava [b], P.S. Negi [a], Muthusamy Prakasam [a], Bahadur Singh Kotlia [c]

[a] Wadia Institute of Himalayan Geology, 33, G.M.S. Road, Dehradun, 248 001, India
[b] Instituto Oceanográfico, Universidade de São Paulo, 191, Praça do Oceanográfico, São Paulo, 05508-120, Brazil
[c] Department of Geology, Kumaun University, Nainital, 263 001, India

ARTICLE INFO

Article history:
Received 10 August 2020
Received in revised form
23 January 2021
Accepted 25 January 2021
Available online 9 February 2021

Handling Editor: P Rioual

Keywords:
Middle Holocene
Indian summer monsoon
Cultural changes
Himalaya
Multi-proxy

ABSTRACT

Agriculture is a major contributor to the economic development of modern as well as ancient India and largely depends on the rainfall in the monsoon season. In order to understand the impact of climate variability on cultural changes in the Indian subcontinent, high resolution centennial to millennial scale middle Holocene Indian summer monsoon (ISM) variability was reconstructed from Bednikund lake, located in an alpine meadow of the Pindar basin, Chamoli, Central Himalaya. Increased ISM precipitations were found during ~5930-3950 (mid-Holocene climate optimum), ~3380–2830 (Minoan Warm Period), ~2610–1860 (Roman Warm Period), ~1050–760 (Medieval Climate Anomaly), and ~320 cal yr BP to Present (Current Warm Period). The decreased ISM strengths were found during ~3950-3380, ~2830–2610, ~1860–1050 (Dark Ages Cold Period), ~760–580, and ~500-320 cal yr BP (Little Ice Age). The covariance between our records of precipitation change and total solar irradiance for the middle to late Holocene and with Northern hemisphere (NH) temperature for the past two millennia suggested solar insolation as a primary forcing mechanism of ISM variability. The reconstructed paleoclimate combined with archaeology and historical records indicated that ancient Indian civilizations e.g., the Indus Valley (~5200-3300 cal yr BP) and Vedic (~3400-2400 cal yr BP) had established and thrived during periods of strengthened ISM precipitation, whereas their collapse closely corresponded to the decreased strength in ISM. From ~2400 to 200 cal yr BP, the Indian subcontinent witnessed the rise and fall of various Kingdoms/dynasties. This period saw an exponential expansion/growth in agriculture, economy, population, languages, architecture, and religions in the Indian subcontinent. The agrarian-based economy showed little or no impact of monsoon weakening after ~2400 cal yr BP possibly due to development and reforms in administrative policies, construction of irrigation systems such as dams, lakes and canals, use of technology for irrigation such as waterwheel, knowledge of double cropping, production of cash crops. The ancient civilizations of India were directly impacted by the strengthening and weakening of ISM, whereas for the later periods, civilizations were able to adapt to climate change.

1. Introduction

The Himalaya is home to numerous glaciers, lakes and rivers that comprise the vast landscape of the Indian subcontinent and host a fragile ecosystem. The Indian summer monsoon (ISM) and westerlies are often linked with the dynamics of Himalayan glaciers, lakes, and rivers. The ISM is a primary freshwater source for agriculture in south Asian countries. The variations in ISM precipitation results in severe droughts and floods affecting the societal and economic balance of roughly a quarter of the world's population. Several famines that killed millions of people in India during the 18th and 19th centuries were linked to the monsoon failures (Grove, 2006; Cook et al., 2010; Mishra et al., 2019). The rise and fall of past civilizations in the Indian subcontinent during the middle Holocene has also been linked to variations in ISM strength (Dixit et al., 2014, 2018; Kathayat et al., 2017; Dutt et al., 2019). For example, the Indus Valley/Harappan civilization flourished during intensified monsoon rainfall between ~5000 and 4400 cal yr BP,

* Corresponding author. Wadia Institute of Himalayan Geology, 33, G.M.S. Road, Dehradun, 248 001, India.
E-mail address: rsuman26@gmail.com (S. Rawat).

https://doi.org/10.1016/j.quascirev.2021.106825
0277-3791/

whereas prolonged drought after ~4400 cal yr BP led to an eastward migration of the population (Dixit et al., 2018).

The ISM is a complex climatic system sensitive to solar forcing, oceanic and atmospheric dynamics (Gupta et al., 2003; Kaushal et al., 2018). The strengthening (/weakening) of ISM is commonly linked with the northward (/southward) shift of the Intertropical Convergence Zone (ITCZ) during periods of high (/low) Northern Hemisphere (NH) insolation (Kutzbach, 1981; Haug et al., 2001; Fleitmann et al., 2003, 2007; Wang et al., 2005). Decadal to centennial-scale variability in the ISM strength is also linked with the El-Niño Southern Oscillation (ENSO)-like and North Atlantic Oscillation (NAO)-like conditions (Moy et al., 2002; Gupta et al., 2003; Rein et al., 2005; Wang et al., 2005).

Lakes effectively record changes in the local environment (e.g., productivity, sediment supply, and nutrient dynamics) that may be largely governed by variations in regional and global climate. On the Indian subcontinent, the majority of Holocene climatic records from lakes have poor to moderate resolution, either due to poor chronological control or coarse sampling resolution. Further, limited high resolution studies on lake sediments from different basins have shown inconsistency in centennial to millennial-scale climate possibly due to variations in precipitation patterns across the different basins. Speleothem records provide high-resolution data of ISM precipitation, however, only a limited number of studies from a spatially very large Himalayan range has been carried out (e.g., Berkelhammer et al., 2012; Dutt et al., 2015; Kotlia et al., 2015; Kathayat et al., 2016, 2017). As a result, extreme events and abrupt changes in ISM precipitation during the middle to late Holocene in Himalaya are still poorly understood. Modern climatic data on extreme weather conditions over the last ~100 years have shown large-scale damages in socio-economic conditions of India through floods and droughts (De et al., 2005). The fragile ecosystems of Himalaya have become more vulnerable to the extreme ISM precipitation events triggering extensive landslides and glacial-lake outbursts (Bhambri et al., 2016). Climate predictions for the 21st century have shown the possibility of an increase in heavy rainfall events (Sharmila et al., 2015), which might lead to more economic and societal damages in the Himalayan regions.

Here, we reconstructed middle Holocene (~6000 cal yr BP) to present (i.e., 1950 CE) ISM variability using a multi-proxy record from high altitude Bednikund lake in the Pinder basin of the central Himalaya. The Bednikund lake is en-route to the pilgrimage track of Roopkund lake (also known as skeleton lake) and the Nanda Devi shrine. A recent study on a DNA and AMS ^{14}C chronology of several human skeletons from Roopkund lake suggested that at least two catastrophic events registered at around ~800 and 1800 CE has led to the demise of travelers (Harney et al., 2019). However, a detailed and long-term paleoclimatic record for these regions has not yet been produced. Therefore, it is important to have a multi-proxy paleoclimate record from such areas to understand the extreme events of the past. The Bednikund lake and catchment soil samples were studied using organic geochemical proxies, particle size, and environmental magnetism. The reconstructed paleoclimate was compared with regional paleoclimate data and forcing factors to understand the climate dynamics and cultural changes in the Indian subcontinent over the past ~6000 cal yr BP.

2. Study area

The Bednikund lake lies in the high altitude alpine meadow (locally termed as "Bugyal") region of Bedni Bugyal (~3350–3800 m a.s.l.; N 30.2061° - 30.2025°, E 79.6572° - 79.6600°), located above the modern-day *tree line* in the Pindar basin of Chamoli, Uttarakhand Himalaya (Fig. 1a and b). The Bedni meadow spreads over an area of ~20 km^2 and falls in the Nanda Devi Biosphere Reserve. The Bednikund lake has an area of ~0.018 km^2. The Bednikund lake is a pilgrim site for Hindus and every 12 years a procession known as the Nanda Devi Raj Jat Yatra goes through Bednikund to Roopkund and Nanda Devi shrine. Since, it's a pilgrim site, part of the shoreline of Bednikund lake has been artificialized with concrete (Fig. 1c). Further, due to its scenic beauty, thousands of trackers camp every year in and around the Bedni meadow during the summer months of May–July. The tree line vegetation in the region is dominated by fir, birch, and rhododendron. The alpine vegetation of Bedni meadow is mostly composed of *Primula*, Brahma kamal, Cyperaceae, *Anemones*, *Potentilla*, lousewort, wild *Salvia,* and thistles (Naithani, 1984). The study area has crystalline rocks of the Munsiari Formation, Lesser Himalaya and of the Vaikrita Group, Higher Himalaya. The main rock types in and around the study area is comprised of low to medium grade metamorphic rocks like granite-granodiorite and augen gneiss of the Munsiari Formation and high-grade metamorphic rocks like kyanite gneiss, staurolite, quartzite, garnet, and biotite schist of the Vaikrita Group (Srivastava and Ahmad 1979; Valdiya, 1980). The catchment soils can be broadly classified into alpine-meadow soils.

The climate data of Chamoli district from 1901 to 2002 CE were acquired from an online meteorological data source (https://www.indiawaterportal.org/met_data/) (Fig. 1d). The annual minimum and maximum temperatures during summer (May–June) and winter (December–January) seasons varies from ~13.2–28.5 °C (mean = 22 °C) and ~2.2–17.9 °C (mean = 16.6 °C), respectively (Fig. 1d). The annual rainfall in the region varies from ~8 to 295 mm (mean = 94 mm). Maximum rainfall (~80%) occurs during the summer monsoon season (June–September), whereas minimum rainfall (~17%) occurs during the winter season (October–February) (Fig. 1d). Western circulation precipitates as snowfall during the month of January and February.

3. Materials and methods

3.1. Sample collection

We trenched two sites outside of the artificial concrete boundary of the Bednikund lake to avoid any anthropogenic disturbances (Fig. 1c). The ~125 and 197 cm deep pits were dug from these two sites namely BBK (N 30.2060°, E 79.6661°) and B_KUND (N 30.2065° E 79.6680°), respectively (Fig. 1c). In ~125 cm deep BBK profile, the top 116 cm sedimentary profile was composed of silt and clay, whereas clasts of pebbles and gravels supported by silt-clay matrix were encountered below 116 cm depth (Supplementary Fig. S1a). The samples from the BBK profile were collected at every 1 cm interval up to 116 cm depth for high-resolution multi-proxy analyses. The distinct organic matter rich black colored layers were seen at different depth intervals in the BBK profile (Supplementary Fig. S1a). In ~197 cm deep B_KUND profile, similar lithological variations were observed with distinct black layers (Supplementary Fig. S1b). The samples from these organic matter rich black layers in the B_KUND profile were also collected for depositional and chronological comparisons. We also collected 11 modern soil (~0–5 cm depth) samples from the catchment area for sediment source characterization and modern vegetation productivity in the study area (Fig. 1c).

3.2. Radiocarbon dating

A total of seven organic matter rich dry bulk sediment samples from BBK and four samples from B_KUND profiles were dated at Poznan Radiocarbon Laboratory, Poland and Woods Hole

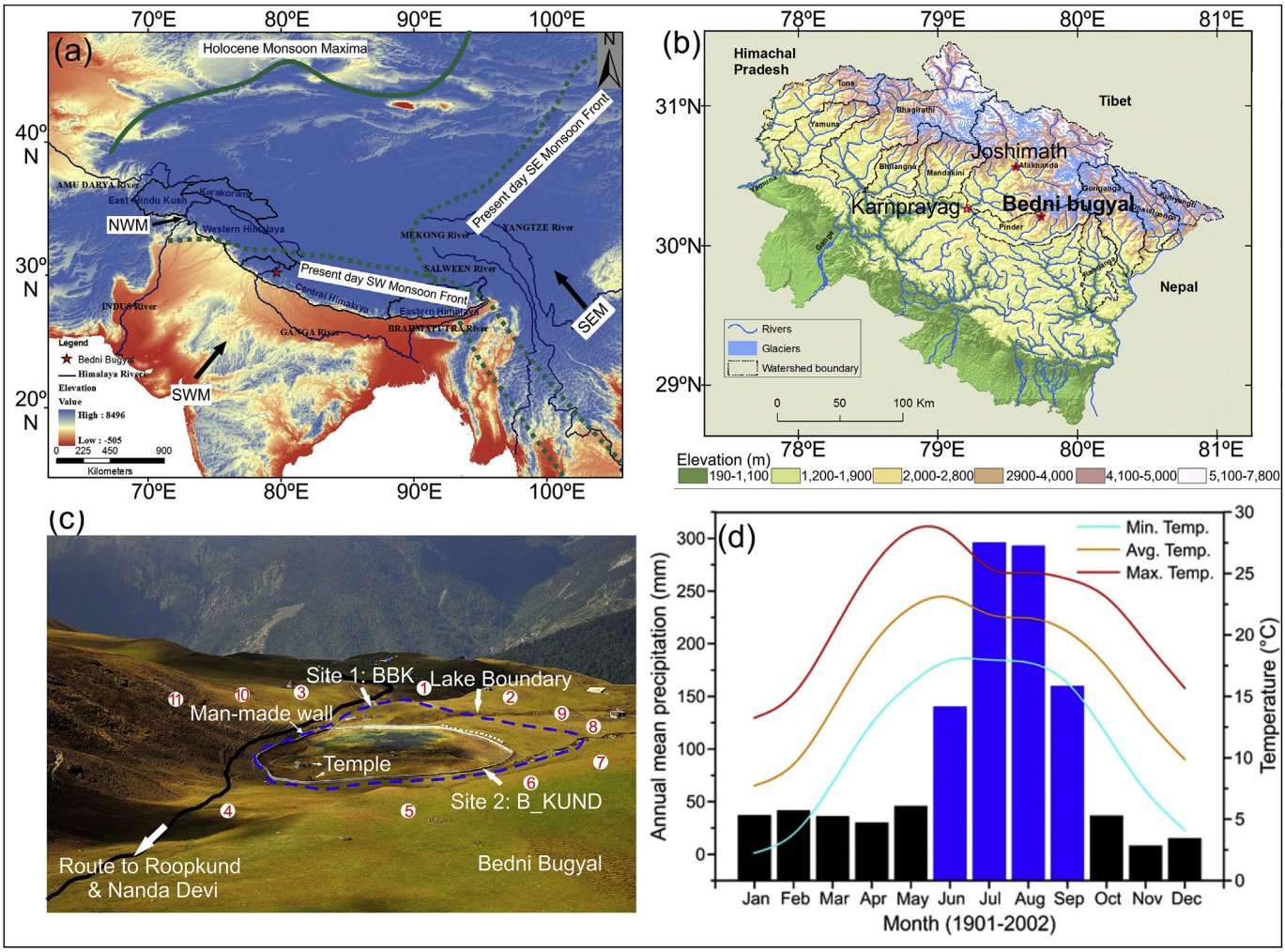

Fig. 1. (a) The Asian monsoonal settings and location of study area. (b) Watershed boundaries of Garhwal Himalaya. (c) Field photograph of Bednikund lake showing BBK and B_KUND sites and catchment soil sample locations (1-11). (d) Climatograph of Chamoli.

Table 1
The AMS^{14}C results of the BBK profile obtained from the Poznan Radiocarbon Laboratory, Poland (Lab numbers with PoZ) and Woods Hole Oceanographic Institute, U.S. (Lab number with OS).

Sample Id	Depth (cm)	Lab number	Sample type	AMS^{14}C Ages (yr BP)	Minimum Age (cal yr BP)	Maximum Age (cal yr BP)	Median Age (cal yr BP)
BBK-16	16	Poz-92967	Bulk sediment	245 ± 30	152	399	288
BBK-34	34	Poz-92968	Bulk sediment	460 ± 30	465	617	515
BBK-53	53	OS-113776	Bulk sediment	1090 ± 15	944	1055	991
BBK-84	84	OS-113777	Bulk sediment	1870 ± 20	1741	1890	1832
BBK-95	95	OS-113778	Bulk sediment	2840 ± 20	2859	3052	2940
BBK-105	105	Poz-93531	Bulk sediment	3630 ± 35	3816	4133	3950
BBK-116	116	OS-113779	Bulk sediment	5180 ± 20	5770	5994	5931

Oceanographic Institute, USA using an AMS^{14}C dating technique (Table 1 and Supplementary Table S1). A detailed description of the sample treatment, processing and method of AMS^{14}C dating can be accessed from respective websites of the laboratories https://radiocarbon.pl/en/and https://www.whoi.edu/nosams/home. The calibration of radiocarbon ages (using IntCal13 data set) and construction of the age-depth model was carried out using the Bacon package (version 2.3.9.1) in R software (version 3.4.2) (Fig. 2a) (Blaauw and Christen, 2011; Reimer et al., 2013).

3.3. Grain size

Grain size analysis of 116 samples from BBK profile was carried out using a Malvern Mastersizer 2000 laser particle size analyzer at Wadia Institute of Himalayan Geology (WIHG). Approximately 1.5 g of each oven-dried (~50 °C) sample were pretreated with 20 ml of 30% H_2O_2 and 10 ml of 10% HCl to remove the organic and carbonate matters, respectively. After each acid treatment, the samples were rinsed multiple times (until pH become neutral) with distilled water and centrifuged at 5000 rpm for 5 min to remove the acidic ions. The grain size distribution was measured with 100 bins

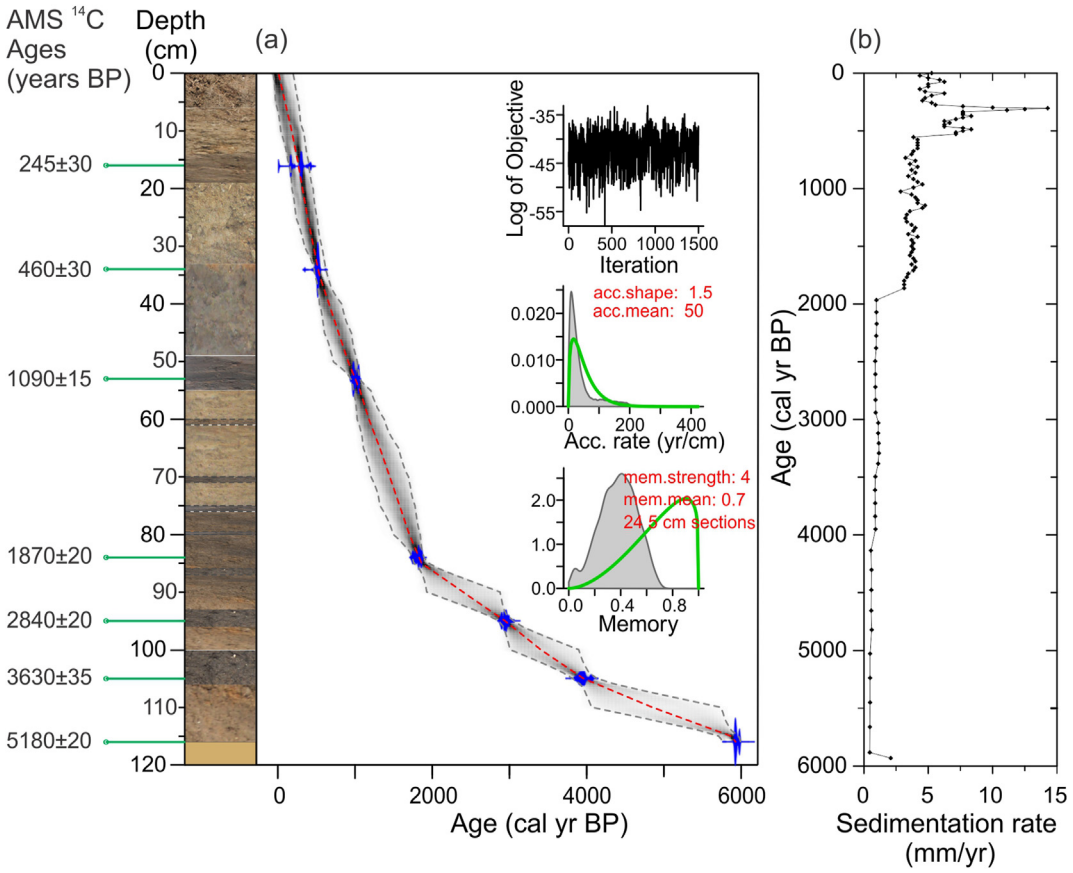

Fig. 2. (a) Bacon age-depth model with calibrated ages shown in blue. The dotted lines (grey) indicate the 95% confidence limits and the dashed line (red) shows the weighted median ages for each depth. (b) Age vs. sedimentation rate. (For interpretation of the references to color in this figure legend, the reader is referred to the Web version of this article.)

ranging from 0.02 to 2000 μm with an obscuration level of 10 ± 3%.

A powerful statistical approach known as end-member modelling analysis (EMMA) was applied on grain size distributions (GSD) data using the Matlab software with the AnalySize package (Paterson and Heslop, 2015). The preferred number of end-members were chosen to determine the distinct subpopulations in the grain size components of sediments. For paleoclimatic studies, this modelling is widely used to infer the underlying sediment sources, transport mechanisms, and post-depositional process in various sedimentary archives like marine, lacustrine and aeolian (Jiang et al., 2017; Liu et al., 2019; Yu et al., 2019; Hateren et al., 2020; Liang et al., 2020).

3.4. Environmental magnetism

All samples from the BBK profile and catchment soils were analyzed for magnetic susceptibility (χ), saturation isothermal remanent magnetization (SIRM), and coercivity of remanence (B_{CR}) to determine the magnetic mineralogical and concentration variations. χ was measured in 0.46 kHz frequency using a Bartington MS2B laboratory sensor. SIRM was imparted at 2200 mT forward field using an ASC Scientific Impulse magnetizer (IM-10). The remanence was measured using a Molspin spinner fluxgate magnetometer. B_{CR} was measured using a backfield remanence curve. B_{CR} is commonly used to distinguish low coercivity ferrimagnetic minerals (e.g., B_{CR} <70 mT for magnetite) and high coercivity antiferromagnetic minerals (e.g., B_{CR} ~30–821 mT for hematite) (Peters and Dekkers, 2003). χ and SIRM data were mass normalized. All the magnetic measurements were carried out at WIHG.

3.5. Organic geochemistry

Stable organic carbon isotope ($\delta^{13}C_{org}$) of BBK lake sediments and catchment soils were measured using an Elemental Analyzer (Flash EA, 2000) coupled with a Delta V plus Continuous Flow Isotope Ratio Mass Spectrometer (CF-IRMS), Thermo Scientific through ConFlow IV at WIHG. For $\delta^{13}C_{org}$ measurement, ~1 g of homogenized fine powdered samples were treated with 0.6 N HCl to remove the carbonate content. Subsequently, samples were rinsed repeatedly with Milli-Q water and centrifuged to remove acid and soluble salts. The samples were then oven-dried at 50 °C and again fine powdered prior to $\delta^{13}C_{org}$ analysis. Then powdered samples were weighed and packed into ultra-cleaned pressed tin capsules for $\delta^{13}C_{org}$ measurements. Total nitrogen (TN) content was measured on non-acid treated bulk powdered samples. The TN content was calculated from the peak area obtained from the sum of integrated m/z 28 and 29 signal measured on bulk samples in CF-IRMS (Jensen, 1991). International (IAEA-CH_3, USGS-32 KNO_3 and ACA) and in-house standards (Sigma-Aldrich glucose, KNO_3) were also analyzed before and after every six samples to calibrate the reference gas and carbon isotopic data, and to check the accuracy of the isotopic measurements with an external precision of ±0.1‰ (1σ). The reproducibility of data was also checked by repeated measurements of samples.

The total organic carbon (TOC) was measured on ~10–20 mg

oven-dried (~60 °C) finely powdered samples using a Shimadzu SSM-5000 A attached with a TOC-LCPH analyzer at WIHG. The instrument functions on the principle of oxidation through heating and combustion and measures the concentration of total carbon (TC) and total inorganic carbon (TIC). The TOC was calculated as a difference between TC and TIC and presented in weight percentages.

4. Results

4.1. Bednikund lake

4.1.1. Lithology, age-depth model and sediment accumulation rate

The BBK and B_KUND sites were dug to understand the lithological variations and sedimentation history of the Bednikund lake. The detailed lithological comparison of both profiles are provided in Supplementary Fig. S1. The BBK and B_KUND profiles showed significant sediment color variation from light yellow to dark brown along with distinct characteristic black layers at different depths (Supplementary Fig. S1). These characteristic black layers are rich in clay and organic matter. The depth intervals other than black layers contain mostly clay, silt, and sand fractions. The B_KUND profile showed relatively coarser grained texture with the appearance of big clasts at the top of the lake sequence compared to the BBK profile. This textural variation is possibly due to the location of the B_KUND site in the peripheral area close to stream inlets supplying high energy deposits (Fig. 1c). A strong lateral variation in lake sediment is not uncommon (Boyle, 2002). In general, the depocenter of lakes receives higher sedimentation compared to the marginal peripheral regions of the lakes (Wang et al., 2009). In the present studied sections, B_KUND profile received higher sedimentation than BBK profile due to its proximity to the source of sediment supply. However, we chose the BBK profile for a detailed paleoclimatic investigation as it possess the most complete stratigraphy.

The sedimentation history of Bednikund lake was established using seven AMS ^{14}C dates from BBK profile (Table 1; Fig. 2). The ages of individual sediment depth horizons at each cm interval were based on interpolated weighted median age calculated from Bacon analysis (Supplementary Table S2). All AMS ^{14}C ages were in stratigraphic order indicating continuous sedimentation. Sediment accumulation rate (SAR) varied from ~0.05 to 1.43 mm yr^{-1} (Fig. 2b). Four distinct sediment accumulation phases were identified in the Bednikund lake age model (Fig. 2b). (1) Low sedimentation: ~0.09 mm yr^{-1} during ~5930 to 1860 cal yr BP; (2) medium sedimentation: ~0.39 mm yr^{-1} during ~1860 to 515 cal yr BP; (3) high sedimentation: ~0.84 mm yr^{-1} during ~515 to 288 cal yr BP, and (4) medium sedimentation: ~0.53 mm yr^{-1} during ~288 cal yr BP to present (Fig. 2b).

4.1.2. Grain size

Grain size analysis of the BBK sediments showed variations in fine clay (<2 μm), silt (2–62 μm) and sand (>62 μm) fractions from ~0.9 to 10% (average = 5%), ~33–86% (average = 67%) and ~8–66% (average = 28%), respectively (Rawat et al., 2021 Mendeley Data: Table 1). Grain size numerical un-mixing results showed three end-members EM1, EM2 and EM3 with mean grain sizes of ~10, 50 and 94 μm, respectively (Fig. 3 and Table 2). The proportions of EM1, EM2, and EM3 varied from ~11 to 91% (average = 51%), 0–63% (average = 32%) and 0–74% (average = 17%), respectively (Table 2).

The EM1 (clay and fine silt) and EM2 (coarse silt) showed opposite behavior throughout the profile except for the last ~500 cal yr BP. A gradual increasing trend in EM1 occurred from ~5930 to 1860 cal yr BP (Fig. 4). Short intermittent periods from ~3950 to 3380 and ~2830 to 2610 cal yr BP showed decreases in EM1 (Fig. 4). Increases in EM2 and decreases in EM1 proportions were recorded from ~1860 to 1050 and ~760 to 580 cal yr BP (Fig. 4). The periods from ~1050 to 760 and ~580 to 500 cal yr BP were characterized by increasing EM1 proportions (Fig. 4). The minimum percentage of EM1 and maximum EM3 (sand) percentage in the entire profile occurred between ~500 and 320 cal yr BP. During this period EM2 proportions had also decreased. From ~320 cal yr BP to Present, proportions of EM1 and EM2 showed increasing trends, whereas EM3 decreased.

4.1.3. Environmental magnetism

The magnetic concentration parameters χ and SIRM co-varied through almost the entire BBK profile (Fig. 4). B_{CR} for BBK profile samples ranged between 11 and 199 mT indicating mixed low coercive (ferrimagnetic) and high coercive (antiferromagnetic) mineral assemblages. SIRM showed a gradually increasing trend between ~5930 and 3380 cal yr BP indicating the increasing concentration of magnetic minerals (Fig. 4). χ had the highest values during this period and showed an almost linear trend up to ~3950 cal yr BP and an increasing trend from ~3950 to 3380 cal yr BP. B_{CR} ranging from ~11 to 22 mT during this interval indicated dominant low coercivity ferrimagnetic mineral assemblage (Rawat et al., 2021 Mendeley Data: Table 2; Fig. 4). From ~3380 to 1860 cal yr BP, a sharp decreasing trend in χ and SIRM was noted suggesting decreased magnetic concentration during this period (Fig. 4). The increased B_{CR} (15–199 mT, average = 129 mT) showed significant presence of high coercivity antiferromagnetic minerals during this period (Fig. 4). A centennial period of increased magnetic concentration was recorded between ~2830 and 2610 cal yr BP. An increasing trend in magnetic concentration parameters between ~1860 and 1050 cal yr BP suggested an overall increased concentration of bulk magnetic minerals (Fig. 4). From ~1050 to 760 cal yr BP decreased concentration of bulk magnetic minerals was found (Fig. 4). B_{CR} varied between ~42 and 123 mT indicating mixed ferri- and antiferromagnetic mineralogy during this period. χ showed increased values for periods (1) ~760 to 580 cal yr BP and (2) ~500 to 320 cal yr BP, whereas values decreased from ~580 to 500 cal yr BP (Fig. 4). From ~320 cal yr BP to present, an overall increased magnetic concentration was found. B_{CR} ranged between ~18 and 51 mT (average = 33 mT) during this period indicating dominant assemblage of low coercivity ferrimagnetic minerals in younger sediments.

4.1.4. Organic geochemistry

The $\delta^{13}C_{org}$ values of Bednikund lake sediments varied between −26.89 and −24.32‰ (VPDB) with an average of −25.54‰ indicating organic matter in lake sediments are from C3 plants (Rawat et al., 2021 Mendeley Data: Table 3; Fig. 4). Several studies based on $\delta^{13}C_{org}$ analysis of modern C3 plant leaves have shown that variations in $\delta^{13}C_{org}$ are mainly explained by the availability of water (mean annual precipitation) (Stewart et al., 1995; Diefendorf et al., 2010; Kohn, 2010; Freeman et al., 2011). Globally, high $\delta^{13}C_{org}$ values of C3 plants are restricted to environments with low mean annual precipitation (Kohn, 2010). Decreasing trends in $\delta^{13}C_{org}$ were recorded for periods ~5930–3950, ~3380–1860, ~1050–760, ~600–510, and ~310 cal yr BP to present (Fig. 4). The periods ~3950–3380, ~1860–1050, ~760–600, and ~510-310 cal yr BP were characterized by increased $\delta^{13}C_{org}$ (Fig. 4).

TOC and TN varied from ~0.35 to 23.51% and ~0.04–1.78%, respectively, indicating highly variable distribution of organic content and nutrients in the lake sediments (Rawat et al., 2021

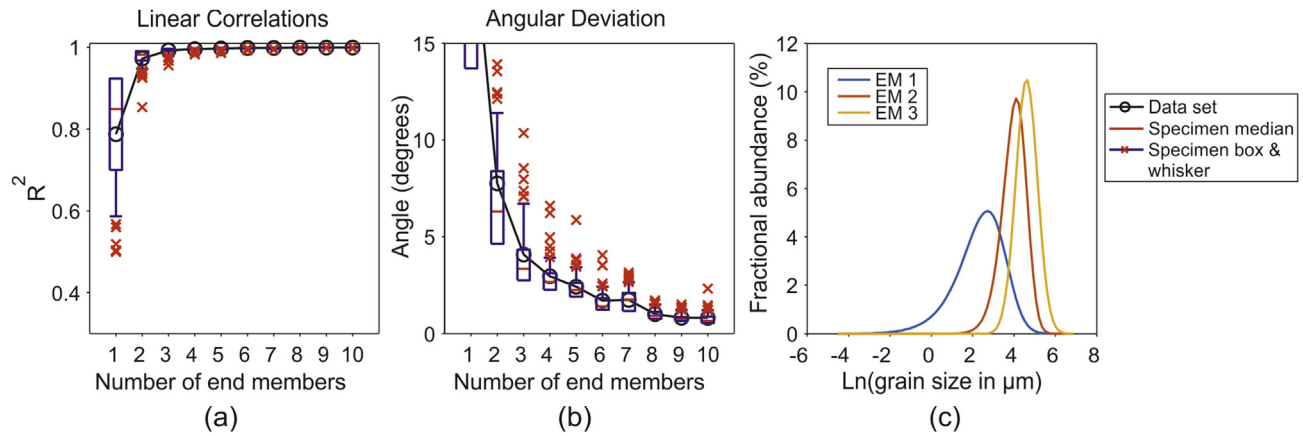

Fig. 3. Results of end-member modelling of grain size data. (a) Linear correlation for each model size class with 1–10 end-members. (b) Angular deviations between reconstructed and observed datasets. (c) Grain-size distributions of the modelled end-members from the selected three end-member model. (For interpretation of the references to color in this figure legend, the reader is referred to the Web version of this article.)

Table 2
Composition of clay, silt and sand fractions for modelled three end-members' results.

End-members	Clay (%)	Silt (%)	Sand (%)	Mean (microns)
EM 1	20.85	76.19	2.95	9.85
EM 2	0.04	62.80	37.16	50.38
EM 3	0	22.09	77.91	93.68

Mendeley Data: Table 3; Fig. 4). TOC and TN showed increasing trends from ~5930–3950, ~3380–1860, ~1050–760, ~600–500 and ~320 cal yr BP to present (Fig. 4). These proxies showed decreasing trends during periods from ~3950–3380, ~2830–2610, ~1860–1050, ~760–600 and ~500-320 cal yr BP (Fig. 4).

4.2. Catchment soils

χ varied from ~1.22 to 2.98 $\times$ 10^{-8} m^3 kg^{-1} (average = 1.92 $\times$ 10^{-8} m^3 kg^{-1}) and SIRM ranged from ~36.22 to 124.23 $\times$ 10^{-5} Am^2 kg^{-1} (average = 63.65 $\times$ 10^{-8} m^3 kg^{-1}) (Rawat et al., 2021 Mendeley Data: Table 4; Fig. 4). B_{CR} ranged from ~10 to 38 mT suggesting presence of low coercivity ferrimagnetic minerals in catchment samples. TOC and TN content varied from ~1.42 to 14.98% (average = 8.03%) and ~0.11–1.38% (average = 0.70%), respectively (Rawat et al., 2021 Mendeley Data: Table 5; Fig. 4). The $\delta^{13}C_{org}$ varied between −24.84 and −25.88‰ (average = −25.37‰) (Rawat et al., 2021 Mendeley Data: Table 5; Fig. 4).

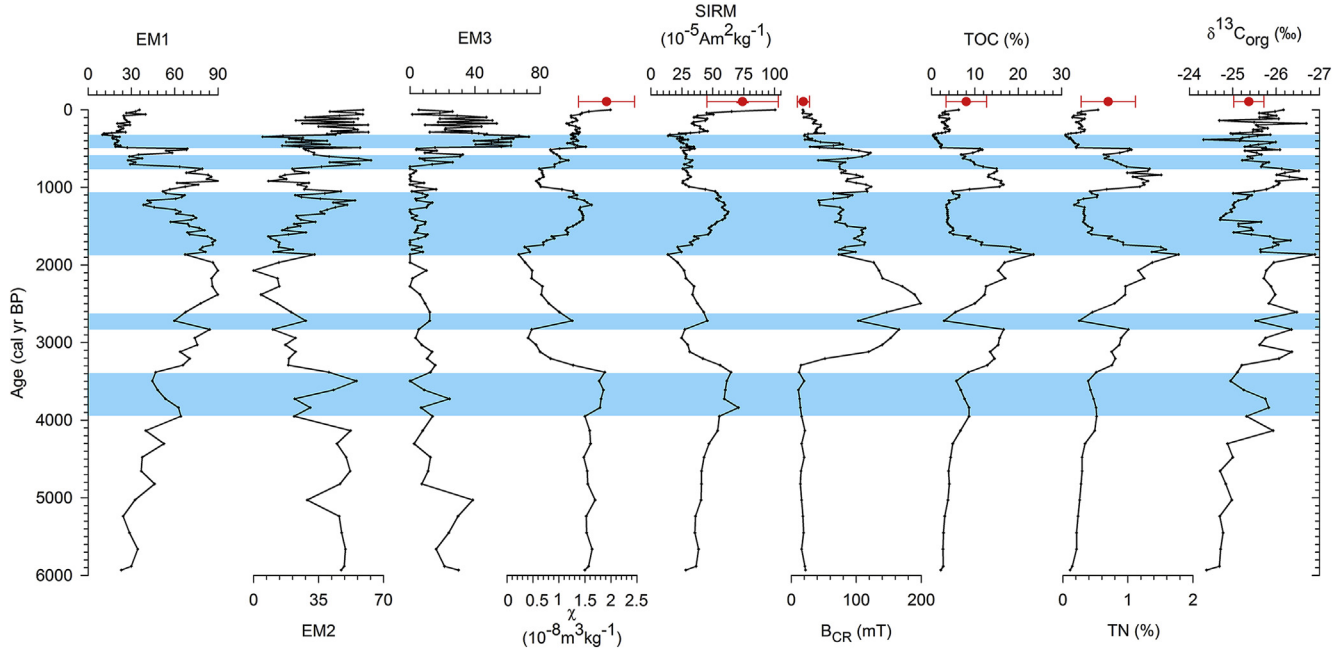

Fig. 4. Temporal variations in grain size end-members (EM1, EM2 and EM3), environmental magnetism (χ, SIRM and B_{CR}) and organic geochemistry (TOC, TN and $\delta^{13}C_{org}$) data of the BBK profile. The circle and line at the top show average and standard deviation of the catchment samples data.

5. Discussion

5.1. Reconstructing local environment

In lacustrine environments, finer sediment fraction suggests higher/deeper lake levels, whereas coarser particles suggest lower/shallower lake levels (Yanhong et al., 2006; Kasper et al., 2012; Bird et al., 2014). The concept is based on hydrological energy and distance of sedimentation from the lake shoreline (Håkanson and Jansson, 1983). During higher lake level, the center of the lake would be more distal from runoff such that only finer sediment particles will be deposited in the center of the lake and coarse sediment particles would be confined to the near shore zone of the lake (Bird et al., 2014). In lower lake level conditions, the center of the lake would be more proximal and coarser particles will be deposited under high energy conditions (Bird et al., 2014). Particle size variations in lake sediments also indicate erosional strength e.g., particle coarsening/fining indicate intensified/weakening erosion strength (Wang et al., 2016). Similarly, increases in TOC indicate higher organic productivity under warmer and wetter climatic conditions, and an increase in TN indicates higher nutrient supply essential for lake productivity (Talbot and Livingstone, 1989; Lerman et al., 1995; Beuning et al., 1997; Rawat et al., 2015a). Further, in the absence or limited effect of post-depositional alterations in lake sediments (e.g., magnetic mineral dissolution, authigenesis of secondary ferrimagnetic minerals greigite and bacterial magnetite), an influx of magnetic minerals in lakes can indicate the strength of surface runoff (Dearing et al., 1981; Oldfield et al., 2003; Rawat et al., 2015b).

EM1 showed positive correlations with TOC and TN suggesting that periods of higher lake productivity corresponded with higher lake-level under warm-wet climatic conditions (Fig. 5). EM2 and EM3 showed a negative correlation with TOC and TN which suggests that during shallow lake level conditions, lake productivity had also declined possibly under drier climatic conditions (Fig. 5). χ showed a moderate positive correlation with SIRM indicating possible paramagnetic mineral contribution in total susceptibility (Lanci et al., 1999) (Fig. 5). Magnetic concentration parameters positively correlate with coarse sediment fractions and negatively with fine sediment fractions and organic matter (Fig. 5). These correlations suggest that under a lower lake level and declined catchment productivity/vegetation growth, magnetic concentrations along with coarser sediments had increased, whereas under higher catchment productivity/vegetation growth magnetic concentrations along with coarser sediments had decreased. The higher vegetation growth/cover in the lake catchment tends to firmly bind the soils leading to lower/weak erosion and thus lower supply of magnetic minerals in lakes in spite of strengthened precipitation (Wang et al., 2016). The negative correlations between magnetic concentrations and organic matter could also be possibly due to dilution of magnetic signals and dissolution of magnetic minerals. Organic matter is diamagnetic in nature and its higher abundance can significantly dilute magnetic signals of sediments (Williamson et al., 1998; Dearing, 1999; Stockhausen and Thouveny, 1999; Rawat et al., 2015b; Srivastava and Jovane, 2020). Further, higher organic carbon along with lower sedimentation favors reducing/anoxic environment in lakes. In such anoxic conditions, fine grain ferrimagnetic minerals tend to dissolve leading to overall low or no ferrimagnetic signals (Snowball, 1993; Williamson et al., 1998; Dearing, 1999; Stockhausen and Thouveny, 1999; Tamuntuan et al., 2015; Wang et al., 2016; Srivastava and Jovane, 2020). The dissolution of fine ferrimagnetic minerals tend to enhance the signal of antiferromagnetic minerals (mostly unchanged from dissolution) (Dearing, 1999; Wang et al., 2016). Therefore, peaks in low magnetic concentration, high organic carbon, and dominance of high coercivity antiferromagnetic minerals (high B_{CR}) at ~2900–2800, ~1800, ~900, and ~500 cal yr BP possibly indicate lake anoxic events/cycles (Fig. 4). These anoxic events also corresponded with higher lake level (high EM1 fraction) suggesting anoxic cycles were related to water-depth.

The time intervals from ~5930–3950, ~3380–2830, ~2610–1860, ~1050–760, ~580–500, and ~320 cal yr BP to present were characterized by increasing trends in EM1, TOC, TN and decreasing trend in $\delta^{13}C_{org}$ suggesting higher lake level and lake and catchment productivity under warm and wet climatic conditions (Fig. 4). The intervening periods ~3950–3380, ~2830–2610, ~1860–1050, ~760–580, and ~500-320 cal yr BP showed decreased TOC, TN and increasing trends in the concentration of magnetic minerals, coarse particles (EM2 and EM3) and $\delta^{13}C_{org}$ indicating shallower lake levels, decreased lake and catchment productivity under drier climatic conditions (Fig. 4). The climatic deterioration from ~500 to 320 cal yr BP was abrupt with ~75% and 79% decline in TOC and TN, respectively, occurred within a decade and a maximum decline reaching up to ~96% and 88%, respectively (Rawat et al., 2021 Mendeley Data Table 3; Fig. 4). This period recorded the highest SAR (0.84 mm yr^{-1}) and maximum EM3 fraction (coarse sand). The abrupt change in grain size, minimum organic productivity and highest SAR marks the sediment-infilling of the Bednikund lake basin.

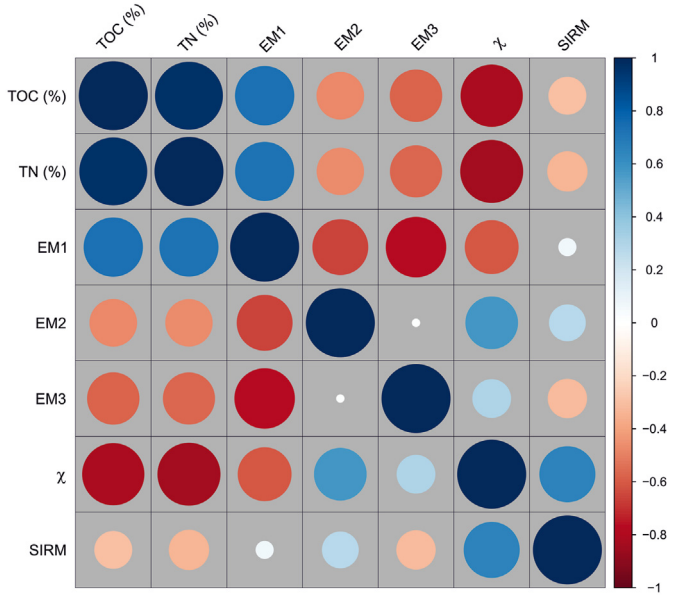

Fig. 5. Correlogram of different grain size end-members, environmental magnetic and organic geochemistry data of the BBK profile. (For interpretation of the references to color in this figure legend, the reader is referred to the Web version of this article.)

5.2. Climate variability and forcing mechanisms

The monsoonal proxies of Bednikund lake strongly mimic total solar irradiance for the middle to late Holocene and NH temperature for the past 2000 years indicating solar insolation as a primary forcing mechanism for the ISM variations (Fig. 6) (Mann and Jones 2003; Steinhilber et al., 2009). Intervals with strengthen ISM precipitation in Bednikund lake were recorded from ~5930–3950, ~3380–2830, ~2610–1860, ~1050–760 and ~320 cal yr BP to present (Fig. 6). These ISM strengthen periods broadly corresponds to the globally warm climatic events i.e., middle Holocene climate optimum (mHCO), Minoan Warm Period (MWP), Roman Warm Period (RWP), Medieval Climate Anomaly (MCA) and Current

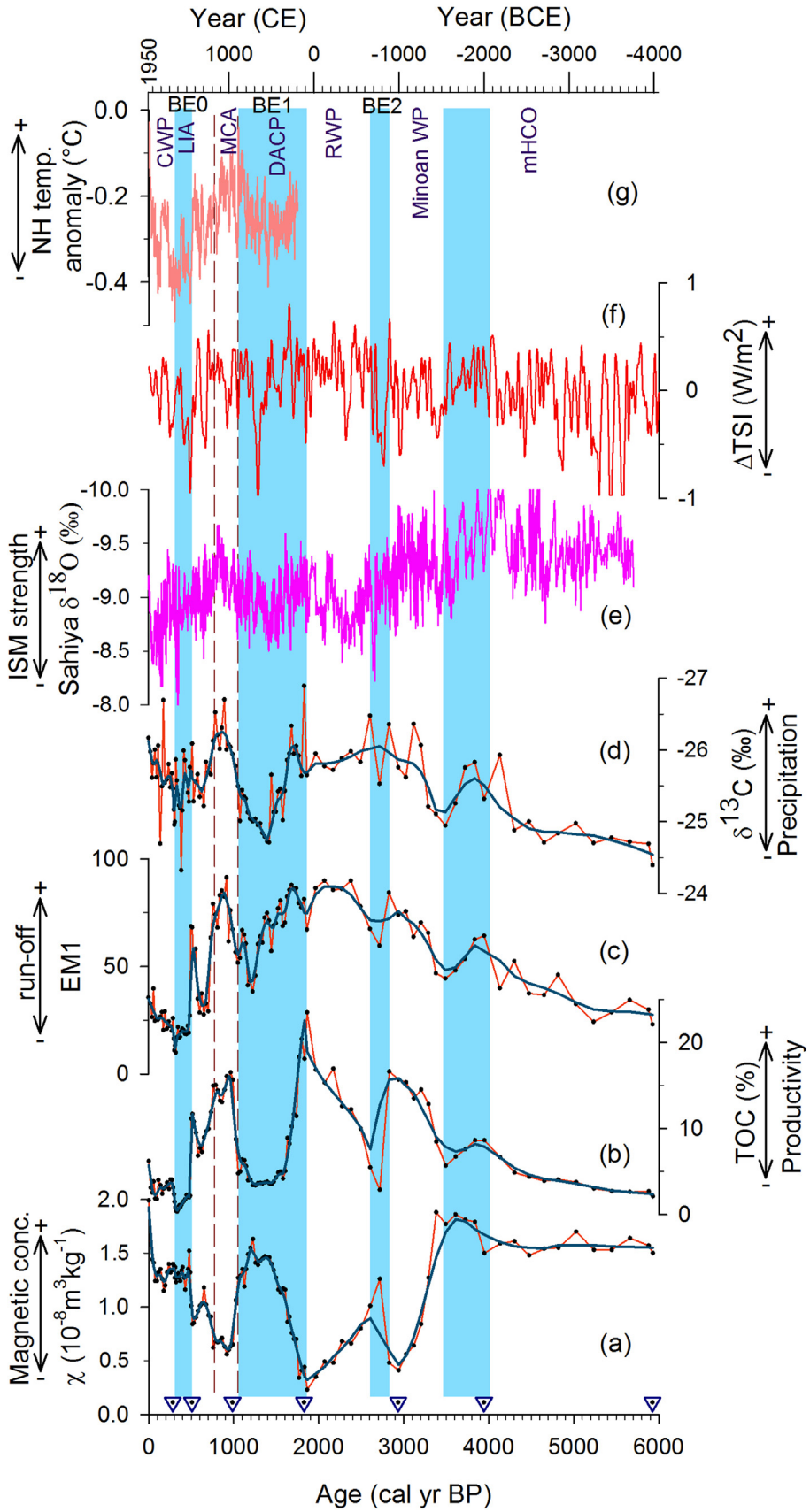

Fig. 6. Comparison of multi-proxy (χ, TOC, EM1 and $\delta^{13}C_{org}$) (a–d) results of Bednikund lake with (e) regional climate record from Sahiya Cave, Garhwal Himalaya (Kathayat et al., 2017), (f) Total solar irradiance (Steinhilber et al., 2009) and (g) NH temperature anomaly (Mann and Jones, 2003). The BE0-BE2 are the North Atlantic Bond events (Bond et al., 2001). The dark blue line overlain on the data represents LOESS smoothing (Factor = 0.055). The inverted triangles show calibrated radiocarbon ages in yr BP.

Warm Period (CWP), respectively (Fig. 6). The weak ISM strength in Bednikund lake was recorded from ~3950–3380, ~2830–2610, ~1860–1050 (Dark Ages Cold Period, DACP), ~760–580, and ~500-320 cal yr BP (Little Ice Age, LIA) (Fig. 6). The weak ISM periods from ~500–320, ~1860–1050, and ~2830-2610 cal yr BP overlaps with the abrupt ocean surface coolings characterized by the Ice-rafted debris (IRD) events in the North Atlantic with peaks at ~500, ~1400, and 2800 cal yr BP (Bond events 0, 1, and 2), respectively (Fig. 6) (Bond et al., 2001). The weak ISM period from ~3950 to 3380 cal yr BP loosely corresponds with the IRD peak at ~4200 cal yr BP (Bond event 3). The weak ISM events recorded during the last ~6000 years corresponded with Bond events revealing the role of North Atlantic teleconnections in the ISM variations.

Recent study by Neukom et al. (2019) found spatial heterogeneity in the timing of temperature maxima during RWP and MCA, and temperature minima during DACP and LIA. They suggested that these climatic periods (RWP, MCA, DACP and LIA) were not globally coherent but rather more regionally. Our record of precipitation change in Bednikund lake co-varies with a regional record of ISM strength from Sahiya Cave, Garhwal (Fig. 6) (Kathayat et al., 2017). The other regional records from different basins of central and NW Himalaya (e.g., Dokriani, Alaknanda, Kumaun, Chandra basin) have also shown similar (with a centennial scale offset in few periods) strengthening and weakening of ISM in the last ~6000 years (Phadtare, 2000; Kotlia and Joshi, 2013; Kotlia et al., 2015; Rawat et al., 2015a, b; Bhushan et al., 2018).

5.3. Climate change and cultural linkages in the Indian subcontinent

The Indian subcontinent flourished with several civilizations (/cultural changes) during the middle to late Holocene. Previous studies have highlighted the significance of climate change in the establishment and demise of various civilizations worldwide (e.g., Hodell et al., 1995; Binford et al., 1997; deMenocal, 2001; Weiss and Bradley, 2001; Haug et al., 2003; Staubwasser et al., 2003; Buckley et al., 2010; Giosan et al., 2012; Dixit et al., 2014; 2018; Kathayat et al., 2017; Sinha et al., 2019). Table 3 provides a summary of the climate and cultural change relationship in the Indian subcontinent over the last 6000 years. The Indus valley civilization (IVC) was a Bronze Age (~5200–3200 cal yr BP) civilization in India (Kenoyer, 1997; Possehl, 2002; Wright, 2010). The IVC is categorized into three development phases as follows (Kenoyer, 1997). (1) Early Harappan Phase (~5200 and 4500 cal yr BP): early regionalization and agriculture-based establishment of the IVC. (2) Mature Harappan Phase (~4500–3900 cal yr BP): development of urban centers/cities. (3) Late Harappan Phase (~3900–3300 cal yr BP): deurbanization of the IVC. Increasing evidence suggests that these three phases of establishment and demise of the IVC are linked with the changes in ISM precipitation. The wet climate (strengthen ISM) during ~5200 to 4500 cal yr BP had been suggested to have facilitated the establishment of agricultural practices in the Early Harappan Phase (Giosan et al., 2012; Dixit et al., 2018; Dutt et al., 2019). By the end of the Early Harappan Phase, urbanization had begun. The surplus in food production during intensified monsoon had possibly led to the development of urban centers (Possehl, 2002; McIntosh, 2007). The weakening of ISM has been suggested to be coincidental with the Mature Harappan Phase when the urbanization was at its peak. However, the initiation of this late Holocene weakening of ISM in various records indicated ages between ~4600 and 3900 cal yr BP (Enzel et al., 1999; Staubwasser et al., 2003; Dixit et al., 2014, 2018; Prasad et al., 2014; Dutt et al., 2018, 2019; Kotlia et al., 2015). Further, several studies suggested that the abrupt nature of the monsoon weakening at ~4200 cal yr BP initiated abandonment (Staubwasser et al., 2003; Dixit et al., 2014) and continued aridity led to deurbanization of the IVC and eastward migration of population in the Late Harappan Phase (Dutt et al., 2019). Irrigation systems during these periods were not developed and this further suggests that agriculture production was mainly dependent on monsoonal precipitation (Giosan et al., 2012). In the present studied climate record, a gradual climate amelioration (warm and humid climate) was found between ~6000 and 3950 cal yr BP corresponding to the Early and Mature Harappan Phases and decreased precipitation conditions from ~3950 to 3380 cal yr BP corresponded to the Late Harappan Phase (Fig. 7). Our findings are consistent and support that the IVC flourished during stable monsoonal precipitation conditions, whereas decreased precipitation and the absence of canal irrigation systems support the hypothesis that a decline in food production led to the demise of the IVC.

After the collapse of the IVC, a second cultural change in the Indian subcontinent is assigned to the Vedic Period when Indo-Aryan people had migrated into NW India and inhabited the Indus valley around ~3400 cal yr BP (Thapar, 1990; Flood, 1996). Unlike the IVC, the Vedic period has not been distinctively classified into different stages of development based on absolute dates but rather more on Vedic texts as well as other archeological evidences (e.g., Painted Grey Ware culture) (Thapar, 1990; Witzel, 1995; Stein, 2010; Trautmann, 2011; McClish and Olivelle, 2012). The Vedic period can broadly be divided into the Early Vedic (~3400–3100 cal yr BP), Middle Vedic (~3100–2800 cal yr BP), and Late Vedic (~2800–2400 cal yr BP) periods (Thapar, 1990; Witzel, 1995). The Early Vedic period is identified as a Late Bronze Age semi-nomadic and pastoral tribal society that initially inhabited in the Indus valley (Thapar, 1990). In the Middle Vedic period, Indo-Aryan people migrated eastward into the fertile land of the Ganga plain. Iron tools (~2900–2400 cal yr BP) were used to clear the forested land of the Ganga plain for agriculture marking the commencement of the Iron Age in India (Stein, 2010). The permanent settling of semi-nomadic and pastoral Indo-Aryan tribes converted into villages/towns. Agriculture led to trade (Thapar, 1990). The Late Vedic period saw an expansion of agriculture, metal, commodity productions and trades, and further eastward migration. The administrative system with a king as its chief was also established (Thapar, 1990). The religious Vedic hymns were composed during this period that became important for Hindu culture. The relationship between climate and culture during the Vedic period is poorly known. Kulke and Rothermund (2004) speculated that the return of higher precipitation after the collapse of the IVC might have prompted immigration of Indo-Aryans in the northern Indus region and declined precipitation around ~2900 cal yr BP led to their eastward migration in the Ganga plain. Recently, Kathayat et al. (2017) also reported that strong ISM prevailed during the Early Vedic period, whereas the weak strength of the ISM at ~3100 cal yr BP corresponded with the eastward migration of Indo-Aryans in the Ganga plain. Kathayat et al. (2017) further reported stable precipitation conditions during the Late Vedic period whereas the abrupt weakening of ISM precipitation coincided with the end of the Vedic period. The present study also found strong ISM precipitation during the Early and Middle Vedic periods (~3400–2800 cal yr BP) and an abrupt decrease in ISM strength in the Late Vedic period (~2800–2600 cal yr BP) (Fig. 7). Our results are consistent with the studies of Kulke and Rothermund (2004) and Kathayat et al. (2017) who postulated that Indo-Aryan immigrated during increased precipitation conditions which might have facilitated agricultural practices. The end of the Vedic period was possibly due to politics, war, cultural and linguistic changes (Witzel, 1987; Kulke and Rothermund, 2004; Kathayat et al., 2017). However, abruptly decreased ISM strength

Table 3
Summary of middle Holocene ISM variability and cultural changes in the Indian subcontinent.

Age (Cal yr BP)	Civilizations/Kingdoms/Dynasties	Key Features	ISM Intensity
5200–4500	Early Harappan Phase	Early regionalization and agriculture based establishment of the IVC	Strengthened ISM
4500–3900	Mature Harappan Phase	Development of urban centers/cities	Strengthened ISM
3900–3300	Late Harappan Phase	Deurbanization of the IVC	Weakened ISM
3400–3100	Early Vedic Period	Migration of late Bronze Age semi-nomadic and pastoral tribal society of Indo-Aryan in Indus valley	Strengthened ISM
3100–2800	Middle Vedic Period	Eastward migration and permanent settling of Indo-Aryans in Ganga plain. Use of iron tools around ~2900 cal yr BP.	Strengthened ISM
2800–2400	Late Vedic Period	Expansion of agriculture, metal, commodity productions and trades and further eastward migration	Abruptly decreased ISM strength between ~2800 and 2600 cal yr BP
~2550–2295	Mahajanapadas	Second urbanization after IVC, land taxes and establishment of trade centers.	Strengthened ISM
~2295–2271	Nanda dynasty	Irrigation projects and canal building	Strengthened ISM
~2271–2135	Maurya Empire	Expansion of agrarian economy, construction of dams, reservoirs, tanks, canals and wells for irrigation. Water tax for irrigation.	Strengthened ISM
~2150–1650	Disintegration of Empire into smaller political regions ruled by Shungas, Satavahanas, Indo-Greeks, Shakas, Kushanas, Cheras and Cholas	Great expansion of trades. Agrarian economy continued to be a source of revenue.	Strengthened ISM up to ~1860 cal yr BP followed by abruptly declined ISM strength.
~1650–1300	Classical Period/Gupta dynasty (*c.* 320–550 CE)	Literature, architecture, science and fine arts had thrived. Maintenance of lakes and dams for irrigation purposes, use of waterwheel for irrigation. Major revenue source was from taxes on land and production. Decline in Roman trade after ~1650 cal yr BP was coincidental with Great Migration Period in Roman Empire and demise of the Western Roman Empire between ~1700 and 1350 cal yr BP.	Weakened ISM
~1300–750	Early Medieval Period: Development of regional states ruled by various Kings/dynasties such as Chauhan, Yadava, Tomara, Chaulukya, Pala, Pandyan, Hoysala, Chola, Pallava and Rashtrakuta.	Fine arts and philosophical system reached its epitome. Agriculture was major source of economy. India witnessed many invasions by Mahmud of Ghazni between ~949 and 924 cal yr BP and by Mu'izz ad-Din Muhammad Ghuri between ~775 and 744 cal yr BP. These invasions for plunder were driven by economic disparity caused by persistent drought in Central Asia during this period whereas Indian economy had flourished under good rainfall conditions.	Strengthened ISM
~744–424	Delhi Sultanate (Mamluk, Khilji, Tughlaq, Sayyid and Lodi dynasties)	Irrigation system was improved with construction of lakes, wells and artificial canals. Market reforms (654-634 cal yr BP) such as establishment of granaries, centralized government-run markets and appointment market controller for strict price controls on grains were introduced. Tax on agriculture land was raised up to 50%. Both population and economy of India had significantly increased.	Weakened ISM for majority of this period.
~424–93	Mughal Empire	Agricultural reforms such as building of imperial irrigation systems had increased produce. Production of cash crops such as cotton, indigo, sugar cane, tree-crops, and opium were promoted under new land revenue system. Extensive road network system connecting towns and cities were constructed to improve the trades. Indian economy contributed ~22–24% of World GDP. Decline in Mughal Empire initiated after ~243 cal yr BP (1707 CE) and ended with establishment of British rule in 93 cal yr BP (1857 CE). Collapse of Mughal Empire and climate crisis (droughts) led a decline in agricultural productivity and deindustrialization in India.	Weakened ISM up to 320 cal yr BP and gradual increase in ISM precipitation afterwards.

during Late Vedic period (~2800-2600 cal yr BP) might have impacted the agricultural production and knowledge of river-based irrigation system might have been known by now (Kulke and Rothermund, 2004).

At the end of the Vedic Period, smaller kingdoms/tribes consolidated into 16 large Kingdoms known as Mahajanapadas (~2550–2295 cal yr BP; *c.* 600-345 BCE). During the Mahajanapadas Period, a second urbanization after the IVC began and true cities were built. Towns grew as a center of industry (such as pottery, carpentry, cloth weaving) and trading centers (Thapar, 1990). The land taxes were collected as revenue for the treasury. The religions Buddhism and Jainism originated and flourished during this period. The Mahajanapadas period was followed by the Maurya Empire that unified the Indian subcontinent in one state for almost 150 years (~2271–2135 cal yr BP; *c.* 321-185 BCE). In the Mauryan Empire, the agrarian economy had expanded greatly. Wastelands were cleared under the direct authority of Kings for new settlements and agricultural expansion. The climate record indicates relatively strengthened precipitation conditions during these periods (Fig. 7). Further, the importance of irrigation for the expansion of agriculture production was well evident in this period. The double cropping was also known by this period. The Nanda dynasty (~2295-2271 cal yr BP; *c.* 345-321 BCE) carried out irrigation projects and build canals. Following this, the Mauryan Empire developed dams, reservoirs, tanks, canals, and wells for irrigation under the Government functionaries (Thapar, 1990). The water tax was

also collected for irrigation in the Mauryan Empire.

After the collapse of the Mauryan Empire, the Indian subcontinent disintegrated into smaller political regions ruled by Shungas, Satavahanas, Indo-Greeks, Shakas, Kushanas, Cheras, and Cholas between ~2150 and 1650 cal yr BP (*c.* 200 BCE and 300 CE) (Thapar, 1990). The agriculture continued to be a source of revenue. However, trade had expanded greatly during this period bringing higher benefits to mercantile communities (Thapar, 1990). The extensive mining of precious stones and metals were also carried out. The expansion of trade also brought cultural dynamism. The architecture/sculptures during this period were centered on Buddhism. Climatically, the period from ~2150 to 1860 cal yr BP witnessed intensified ISM precipitation, whereas the strength of the ISM abruptly decreased from ~1860 to 1600 cal yr BP (Fig. 7).

The period from ~1650 to 1300 cal yr BP (*c.* 300–650 CE) often referred to as a classical period in Indian History when the Gupta Dynasty (*c.* 320–550 CE) ruled over the largest part of the Indian subcontinent except for Deccan and South India (Thapar, 1990). In the Gupta Empire, literature, architecture, science, and fine arts thrived. The crops cultivated during this period had not changed much from previous centuries with growth of the sugarcane and wheat in NW India and rice in the eastern part of the Ganga plain (Thapar, 1990). The use of waterwheels for irrigation purposes was familiar within rural India during this period. Maintenance of previously built lakes and dams were carried out and used for irrigation. The major revenue came from the taxes on land and products, whereas commercial activities did not provide income as large as in the previous period (Thapar, 1990). This is possibly due to the decline of the Roman trade in India after ~1650 cal yr BP (Thapar, 1990). The decline of Roman trade in India coincides with the Great Migration Period in the Roman Empire and the demise of the Western Roman Empire between ~1700 and 1350 cal yr BP (Büntgen et al., 2011). This period witnessed increased climatic variability and political as well as social-economic instability in the Roman Empire (Büntgen et al., 2011). The economic crisis was also evident in the latter part of the Gupta Empire (Thapar, 1990). Climatically, decreased ISM precipitation was recorded during this period (Fig. 7). Therefore, it seems that the economic crisis at the later part of the period was possibly due to the declined trade with Romans and the impact of decreased precipitation on agricultural production.

The early medieval period (~1300–750 cal yr BP; *c.* 650–1200 CE) in India saw developments of regional states ruled by various Kings/dynasties such as Chauhan, Yadava, Tomara, Chaulukya, Pala, Pandyan, Hoysala, Chola, Pallava, and Rashtrakuta. Various temples and monasteries were constructed during this period and many of them are now UNESCO heritage monuments (e.g., Pattadakal monuments). The development in fine arts and the philosophical system had reached new epitomes. Agriculture was one of the large sources of the economy of these dynasties. The NW Indian subcontinent was invaded many times by Mahmud of Ghazni of the Ghaznavid dynasty between ~949 and 924 cal yr BP (*c.* 1001–1026 CE) and by Mu'izz ad-Din Muhammad Ghuri of the Ghurid Empire between ~775 and 744 cal yr BP (1175 and 1206 CE) (Fig. 7). The invasions of Mahmud of Ghazni were for plunder and later invasions of Mu'izz ad-Din Muhammad Ghuri led to the establishment of the Delhi Sultanate between ~744 and 424 cal yr BP (1206–1526 CE). Yadava et al. (2016) suggested that a persistent drought in Central Asia (regions ruled by Mahmud of Ghazni and Mu'izz ad-Din Muhammad Ghuri) occurred between ~850 and 400 cal yr BP (*c.* 1000–1550 CE). This persistent drought might had severely impacted the agro-pastoral economy of these regions, whereas the Indian economy had flourished under fairly good rainfall conditions (Yadava et al., 2016). The economical disparity might had prompted the repetitive and desperate invasions and finally the conquest of India by Mu'izz ad-Din Muhammad Ghuri (Yadava et al., 2016). The motive of previous plunder invasions of India by Mahmud of Ghazni was also to replenish the Ghazni treasury who saw the rich wealth of India and the fertility of the Punjab plains that appeared richer and lush from the barren mountains of the Hindu Kush (Thapar, 1990). During these invasions, warm and wet climate (~1050–760 cal yr BP) prevailed in India that might had facilitated the strengthening of the agrarian economy of India during these periods (Fig. 7). This suggests that climate may have played a role in these invasions.

The Delhi Sultanate (~744-424 cal yr BP) was an Islamic Empire in India ruled by five dynasties (Mamluk, Khilji, Tughlaq, Sayyid, and Lodi dynasties). This period saw significant cultural (Indo-Islamic culture), language (Hindi-Urdu), religion (Islam) and architectural changes (construction of mosques and tombs) in the Indian subcontinent. The irrigation system was improved with the construction of lakes, wells, artificial canals (Siddiqui, 1986). Alauddin Khilji of the Khilji dynasty introduced several market reforms (654-634 cal yr BP) (1296–1316 CE) such as the establishment of granaries, centralized government-run markets and the appointment of market controllers for strict price controls on grains. Alauddin Khilji also raised the tax on agricultural land up to 50% to generate higher revenues (Habib, 1982). India's population and economy had increased significantly between ~950 and 450 cal yr BP (*c.* 1000–1500 CE) of which the Delhi Sultanate period covered a large part (Maddison, 2001). The climate during the majority of this period was characterized by decreased precipitation compared to the early medieval period (Fig. 7).

Zahīrud-Dīn Muhammad Babur defeated the Ibrahim Lodhi of the Delhi Sultanate in 424 cal yr BP (1526 CE) and established the Mughal Empire. The economy during the Mughal Empire was large and prosperous contributing about 22–24% of the World Gross Domestic Product (GDP) at that time (Maddison, 2001). The population grew significantly. The agricultural production during the Mughal Empire had increased due to agricultural reforms such as building of the imperial irrigation systems which led to higher crop yields (Schmidt, 2015). Along with food crop such as wheat, rice, and barley, the production of cash crops such as cotton, indigo, sugar cane, tree-crops, and opium were promoted using land revenue system introduced under the reign of Abul-Fath Jalal-ud-din Muhammad Akbar (394-345 cal yr BP; 1556–1605 CE) (Richards, 1995). An extensive road network system connecting town and cities were constructed to improve the trades. During this period, the Indo-Persian architecture developed and led to the construction of numerous forts/monuments that are UNESCO World heritage sites (e.g., Agra Fort, Red Fort, and Taj Mahal). The decline of the Mughal Empire initiated after ~243 cal yr BP (1707 CE) and ended with the establishment of British rule in 93 cal yr BP (1857 CE). The collapse of the Mughal Empire and climate crisis (droughts) led to a decline in agricultural productivity and deindustrialization in India (Fig. 7) (Clingingsmith and Williamson 2008). Climatically, the majority of the Mughal Empire regime witnessed reduced precipitation condition (Fig. 7). Several drought-led famines during the Mughal Empire have also been reported (Fig. 7) (Uberoi, 2012).

The economy of India from ~1950 to 250 cal yr BP (0–1700 CE) was one of the largest in the world and represented ~22–28% of world GDP (Maddison, 2001). Agriculture had been a major source of economy in ancient as well as in modern India (e.g., ~42–45% share in total India GDP in 1950 CE). Agriculture in the Indian subcontinent largely depends on the seasonal monsoonal rainfall. The above synthesis indicates that the ancient Indus Valley and Vedic civilizations have been directly impacted by variations in monsoonal strength, whereas importance of the irrigation for agriculture was well evident after the Mahajanapadas period.

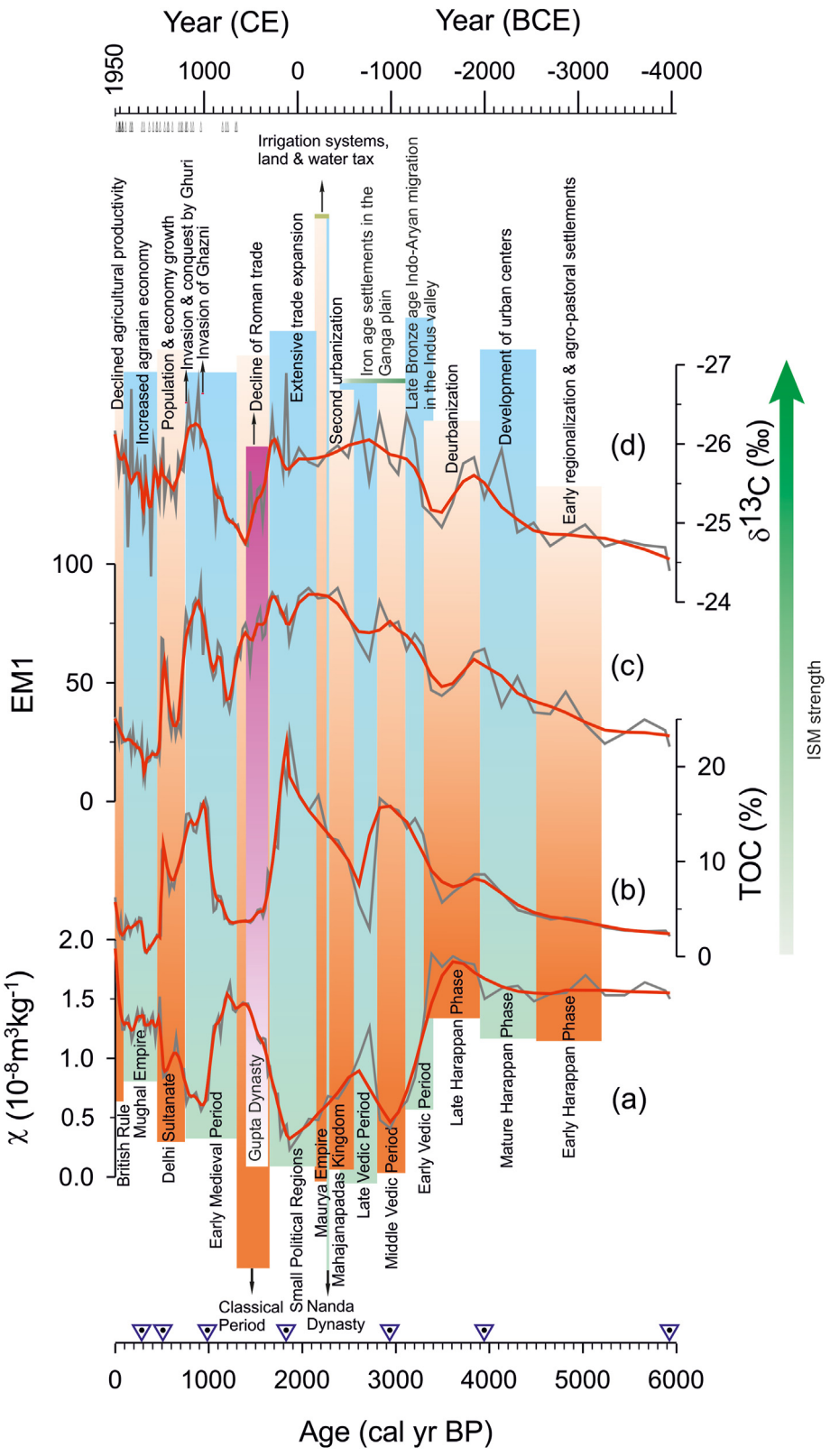

Fig. 7. Climate and cultural relationship over the past ~6000 years in the Indian subcontinent. The small triangles at the top side of the figure mark historical records of droughts and famines (Grove, 2006; Sinha et al., 2007; Uberoi, 2012; Mishra et al., 2019). These droughts and famines are at annual and decadal scales and the thickness of the triangles does not represent ages.

While the agrarian-based Indian economy grew even during periods of reduced precipitation strength, surplus production of food led to the trade and establishment of textile industries. Various irrigation systems such as dams, lakes, and canals were constructed and maintained over the period of time (Pandey et al., 2003), technological advancements such as the use of waterwheel for irrigation, and various agrarian reforms may have reduced the impact of weakened strength of ISM on agriculture. It has to be noted that our study is based on climatic data on centennial to millennial-scale, whereas monsoon failure at an annual/decadal-scale had certainly impacted the society as evidenced by the occurrence of various drought-led famines in the past millennia (Fig. 7) (Grove, 2006; Sinha et al., 2007; Uberoi, 2012; Mishra et al., 2019).

6. Conclusions

1. The multi-proxy data (TOC, $\delta^{13}C_{org}$, EM1, and χ) co-varies with total solar irradiance for the middle and late Holocene and with NH temperature anomaly for the past two millennia indicating solar insolation as a primary forcing mechanisms of ISM variability.
2. Periods of increased ISM strength were found during global warm climate events of mHCO, MWP, RWP, MCA and CWP.
3. Decreased ISM strengths were found during ~3950-3380, ~2830–2610, ~1860–1050 (DACP), ~760–580 and ~500-320 cal yr BP (LIA) and broadly corresponded with Bond events 3, 2, 1, and 0, respectively, indicating North Atlantic teleconnections.
4. The ancient Indian civilizations IVC and Vedic had established and thrived during periods of strengthen ISM precipitation, whereas their collapse closely corresponded to the decreased strength in ISM.
5. The period from ~2400 to 200 cal yr BP witnessed the rise and fall of various kingdoms and dynasties in the Indian subcontinent. This period was also marked by expansion/growth in agriculture, economy, population, languages, architecture, and religions. The agrarian-based economy showed little or no impact on monsoon weakening after ~2400 cal yr BP possibly due to development and reforms in administrative policies, the formation of irrigation systems such as dams, lakes and canals, use of technology for irrigation such as waterwheel, knowledge of double cropping, production of cash crops.
6. The ancient civilizations of India were directly impacted by the strengthening and weakening of ISM, whereas for the later periods, civilizations were able to adapt to climate change.

Declaration of competing interest

The authors declare that they have no known competing financial interests or personal relationships that could have appeared to influence the work reported in this paper.

Acknowledgements

We thank the director of the Wadia Institute of Himalayan Geology for providing necessary working facilities. SR acknowledges Mr. Rakesh Kumar for help in environmental magnetic measurements, Dr. Navya Reghu for Bacon analysis and Dr. Rakesh Bhambri for providing watershed map of the Garhwal basin. We sincerely acknowledge Prof. Luca Lanci and two other anonymous reviewers for their critical and thoughtful reviews which significantly improved the quality of the article. We also acknowledge Prof. Patrick Rioual, Editor, for careful handling of the article. This is Wadia Institute of Himalayan Geology contribution number WIHG/2019/09/01.

Appendix A. Supplementary data

Supplementary data to this article can be found online at https://doi.org/10.1016/j.quascirev.2021.106825.

Credit author statement

Conceptualization: SR, VR and PS; Sampling: SR and PSN; Data curation: VR and SR; Formal analysis: PM and VR did grain size end member modelling. Interpretation: VR and SR interpreted grain size and stable isotope data. PS interpreted environmental magnetic data. BSK helped in data correlation. Writing – original draft: SR, PS and VR wrote original draft. Writing – review & editing: SR and PS. PS wrote cultural change part of paper. Supervision: SR.

Funding

VR acknowledges Wadia Fellowship grant (8/51/2017/-JRF/WIHG/Estt) for financial support. PS acknowledges funding from FAPESP Postdoctoral grant 2019/11364–0. SR acknowledges DST, India project grant ECR/2017/001046.

Data availability

All the data reported in this research article are provided in the manuscript, supplementary files and in Mendeley Data Repository Rawat et al. (2021).

References

Berkelhammer, M., Sinha, A., Stott, L., Cheng, H., Pausata, F.S., Yoshimura, K., 2012. An abrupt shift in the Indian monsoon 4000 years ago. Geophys. Monogr. 198, 75–87.

Beuning, K.R., Talbot, M.R., Kelts, K., 1997. A revised 30,000-year paleoclimatic and paleohydrologic history of Lake Albert, East Africa. Palaeogeogr. Palaeoclimatol. Palaeoecol. 136 (1–4), 259–279.

Bhambri, R., Mehta, M., Dobhal, D.P., Gupta, A.K., Pratap, B., Kesarwani, K., Verma, A., 2016. Devastation in the kedarnath (mandakini) valley, garhwal Himalaya, during 16–17 june 2013: a remote sensing and ground-based assessment. Nat. Hazards 80, 1801–1822.

Bhushan, R., Sati, S.P., Rana, N., Shukla, A.D., Mazumdar, A.S., Juyal, N., 2018. High-resolution millennial and centennial scale Holocene monsoon variability in the Higher Central Himalayas. Palaeogeogr. Palaeoclimatol. Palaeoecol. 489, 95–104.

Binford, M.W., Kolata, A.L., Brenner, M., Janusek, J.W., Seddon, M.T., Abbott, M., Curtis, J.H., 1997. Climate variation and the rise and fall of an Andean civilization. Quat. Res. 47 (2), 235–248.

Bird, B.W., Polisar, P.J., Lei, Y., Thompson, L.G., Yao, T., Finney, B.P., Bain, D.J., Pompeani, D.P., Steinman, B.A., 2014. A Tibetan lake sediment record of Holocene Indian summer monsoon variability. Earth Planet Sci. Lett. 399, 92–102.

Blaauw, M., Christen, J.A., 2011. Flexible paleoclimate age-depth models using an autoregressive gamma process. Bayesian analysis 6 (3), 457–474.

Bond, G., Kromer, B., Beer, J., Muscheler, R., Evans, M.N., Showers, W., Hoffmann, S., Lotti-Bond, R., Hajdas, I., Bonani, G., 2001. Persistent solar influence on North Atlantic climate during the Holocene. Science 294, 2130–2135.

Boyle, J.F., 2002. Inorganic geochemical methods in palaeolimnology. In: Last, M., Smol, J.P. (Eds.), Tracking Environmental Change Using Lake Sediments, vol. 2. Springer, Dordrecht, pp. 83–141.

Buckley, B.M., Anchukaitis, K.J., Penny, D., Fletcher, R., Cook, E.R., Sano, M., Wichienkeeo, A., Minh, T.T., Hong, T.M., 2010. Climate as a contributing factor in the demise of Angkor, Cambodia. Proc. Natl. Acad. Sci. Unit. States Am. 107 (15), 6748–6752.

Büntgen, U., Tegel, W., Nicolussi, K., McCormick, M., Frank, D., Trouet, V., Kaplan, J.O., Herzig, F., Heussner, K.U., Wanner, H., Luterbacher, J., 2011. 2500 years of European climate variability and human susceptibility. Science 331 (6017), 578–582.

Clingingsmith, D., Williamson, J.G., 2008. Deindustrialization in 18th and 19th century India: Mughal decline, climate shocks and British industrial ascent. Explor. Econ. Hist. 45 (3), 209–234.

Cook, E.R., Anchukaitis, K.J., Buckley, B.M., D'Arrigo, R.D., Jacoby, G.C., Wright, W.E., 2010. Asian monsoon failure and megadrought during the last millennium. Science 328 (5977), 486–489.
De, U.S., Dube, R.K., Rao, G.P., 2005. Extreme weather events over India in the last 100 years. Journal of Indian Geophysical Union 9 (3), 173–187.
Dearing, J.A., 1999. Holocene environmental change from magnetic proxies in lake sediments. In: Maher, B.A., Thompson, R. (Eds.), Quaternary Climates, Environments and Magnetism. Cambridge University Press, pp. 231–278.
Dearing, J.A., Elner, J.K., Happey-Wood, C.M., 1981. Recent sediment flux and erosional processes in a Welsh upland lake-catchment based on magnetic susceptibility measurements. Quat. Res. 16 (3), 356–372.
DeMenocal, P.B., 2001. Cultural responses to climate change during the late Holocene. Science 292 (5517), 667–673.
Diefendorf, A.F., Mueller, K.E., Wing, S.L., Koch, P.L., Freeman, K.H., 2010. Global patterns in leaf 13C discrimination and implications for studies of past and future climate. Proc. Natl. Acad. Sci. Unit. States Am. 107 (13), 5738–5743.
Dixit, Y., Hodell, D.A., Petrie, C.A., 2014. Abrupt weakening of the summer monsoon in northwest India ~4100 yr ago. Geology 42 (4), 339–342.
Dixit, Y., Hodell, D.A., Giesche, A., Tandon, S.K., Gázquez, F., Saini, H.S., Skinner, L.C., Mujtaba, S.A., Pawar, V., Singh, R.N., Petrie, C.A., 2018. Intensified summer monsoon and the urbanization of Indus Civilization in northwest India. Sci. Rep. 8 (1), 4225.
Dutt, S., Gupta, A.K., Clemens, S.C., Cheng, H., Singh, R.K., Kathayat, G., Edwards, R.L., 2015. Abrupt changes in Indian summer monsoon strength during 33,800 to 5500 years BP. Geophys. Res. Lett. 42 (13), 5526–5532.
Dutt, S., Gupta, A.K., Singh, M., Jaglan, S., Saravanan, P., Balachandiran, P., Singh, A., 2019. Climate variability and evolution of the Indus civilization. Quat. Int. 507, 15–23.
Dutt, S., Gupta, A.K., Wünnemann, B., Yan, D., 2018. A long arid interlude in the Indian summer monsoon during~ 4,350 to 3,450 cal yr BP contemporaneous to displacement of the Indus valley civilization. Quat. Int. 482, 83–92.
Enzel, Y., Ely, L.L., Mishra, S., Ramesh, R., Amit, R., Lazar, B., Rajaguru, S.N., Baker, V.R., Sandler, A., 1999. High-resolution Holocene environmental changes in the thar desert, northwestern India. Science 284 (5411), 125–128.
Fleitmann, D., Burns, S.J., Mangini, A., Mudelsee, M., Kramers, J., Villa, I., Neff, U., Al-Subbary, A.A., Buettner, A., Hippler, D., Matter, A., 2007. Holocene ITCZ and Indian monsoon dynamics recorded in stalagmites from Oman and Yemen (Socotra). Quat. Sci. Rev. 26 (1–2), 170–188.
Fleitmann, D., Burns, S.J., Mudelsee, M., Neff, U., Kramers, J., Mangini, A., Matter, A., 2003. Holocene forcing of the Indian monsoon recorded in a stalagmite from southern Oman. Science 300 (5626), 1737–1739.
Flood, G., 1996. An Introduction to Hinduism. Cambridge University Press, Cambridge.
Freeman, K.H., Mueller, K.E., Diefendorf, A.F., Wing, S.L., Koch, P.L., 2011. Clarifying the influence of water availability and plant types on carbon isotope discrimination by C3 plants. Proc. Natl. Acad. Sci. Unit. States Am. 108 (16), 59–60.
Giosan, L., Clift, P.D., Macklin, M.G., Fuller, D.Q., Constantinescu, S., Durcan, J.A., Stevens, T., Duller, G.A., Tabrez, A.R., Gangal, K., Adhikari, R., 2012. Fluvial landscapes of the Harappan civilization. Proc. Natl. Acad. Sci. Unit. States Am. 109 (26), 1688–1694.
Grove, R.H., 2006. The great El Niño of 1789–93 and its global consequences: reconstructing an extreme climate event in world environmental history. Mediev. Hist. J. 10, 75–98.
Gupta, A.K., Anderson, D.M., Overpeck, J.T., 2003. Abrupt changes in the asian southwest monsoon during the Holocene and their links to the north atlantic ocean. Nature 421 (6921), 354–357.
Habib, I., 1982. Northern India under the sultanate: agrarian economy. In: Habib, Irfan (Ed.), Tapan Raychaudhuri. CUP Archive, ISBN 978-0-521-22692-9. The Cambridge Economic History of India, c.1200-c.1750.
Håkanson, L., Jansson, M., 1983. Principles of Lake Sedimentology. Springer-Verlag, Berlin, Germany.
Harney, É., Nayak, A., Patterson, N., Joglekar, P., Mushrif-Tripathy, V., Mallick, S., Rohland, N., Sedig, J., Adamski, N., Bernardos, R., Broomandkhoshbacht, N., 2019. Ancient DNA from the skeletons of Roopkund lake reveals mediterranean migrants in India. Nat. Commun. 10 (1), 1–10.
Hateren, J.A.V., Buuren, U.V., Arens, S.M., Balen, R.T.V., Prins, M.A., 2020. Identifying sediment transport mechanisms from grain size–shape distributions, applied to aeolian sediments. Earth Surface Dynamics 8 (2), 527–553.
Haug, G.H., Günther, D., Peterson, L.C., Sigman, D.M., Hughen, K.A., Aeschlimann, B., 2003. Climate and the collapse of Maya civilization. Science 299 (5613), 1731–1735.
Haug, G.H., Hughen, K.A., Sigman, D.M., Peterson, L.C., Röhl, U., 2001. Southward migration of the intertropical convergence zone through the Holocene. Science 293 (5533), 1304–1308.
Hodell, D.A., Curtis, J.H., Brenner, M., 1995. Possible role of climate in the collapse of Classic Maya civilization. Nature 375 (6530), 391–394.
Jensen, E.S., Brink, M., 1991. Automated analysis of 15N and total N in plant material and soil. In: International Symposium on the Use of Stable Isotopes in Plant Nutrition, Soil Fertility and Environmental Studies. IAEA, pp. 54–55. STI-PUB-845.
Jiang, H., Wan, S., Ma, X., Zhong, N., Zhao, D., 2017. End-member modeling of the grain-size record of Sikouzi fine sediments in Ningxia (China) and implications for temperature control of Neogene evolution of East Asian winter monsoon. PloS One 12 (10), e0186153.
Kasper, T., Haberzettl, T., Doberschütz, S., Daut, G., Wang, J., Zhu, L., Nowaczyk, N., Mäusbacher, R., 2012. Indian ocean summer monsoon (IOSM)-dynamics within the past 4 ka recorded in the sediments of lake nam Co, central Tibetan plateau (China). Quat. Sci. Rev. 39, 73–85.
Kathayat, G., Cheng, H., Sinha, A., Spötl, C., Edwards, R.L., Zhang, H., Li, X., Yi, L., Ning, Y., Cai, Y., Lui, W.L., 2016. Indian monsoon variability on millennial-orbital timescales. Sci. Rep. 6, 24374.
Kathayat, G., Cheng, H., Sinha, A., Yi, L., Li, X., Zhang, H., Li, H., Ning, Y., Edwards, R.L., 2017. The Indian monsoon variability and civilization changes in the Indian subcontinent. Science Advances 3 (12), e1701296.
Kaushal, N., Breitenbach, S.F., Lechleitner, F.A., Sinha, A., Tewari, V.C., Ahmad, S.M., Berkelhammer, M., Band, S., Yadava, M., Ramesh, R., Henderson, G.M., 2018. The Indian summer monsoon from a speleothem δ18O perspective—a review. Quaternary 1 (3), 29.
Kenoyer, J.M., 1997. Trade and technology of the Indus valley: new insights from harappa, Pakistan. World Archaeol. 29 (2), 262–280.
Kohn, M.J., 2010. Carbon isotope compositions of terrestrial C3 plants as indicators of (paleo) ecology and (paleo) climate. Proc. Natl. Acad. Sci. Unit. States Am. 107 (46), 19691–19695.
Kotlia, B.S., Joshi, L.M., 2013. Late Holocene climatic changes in garhwal Himalaya. Curr. Sci. 911–919.
Kotlia, B.S., Singh, A.K., Joshi, L.M., Dhaila, B.S., 2015. Precipitation variability in the Indian central Himalaya during last ca. 4,000 years inferred from a speleothem record: impact of Indian summer monsoon (ISM) and westerlies. Quat. Int. 371, 244–253.
Kulke, H., Rothermund, D., 2004. A History of India. Routledge Taylor & Francis Group Press, p. 432p.
Kutzbach, J.E., 1981. Monsoon climate of the early Holocene: climate experiment with the earth's orbital parameters for 9000 years ago. Science 214 (4516), 59–61.
Lanci, L., Hirt, A.M., Lowrie, W., Lotter, A.F., Lemcke, G., Sturm, M., 1999. Mineral-magnetic record of Late Quaternary climatic changes in a high Alpine lake. Earth Planet Sci. Lett. 170 (1–2), 49–59.
Lerman, A., Imboden, D.M., Gat, J.R. (Eds.), 1995. Physics and Chemistry of Lakes. Springer-Verlag, Berlin.
Liang, A., Dong, Z., Su, Z., Qu, J., Zhang, Z., Qian, G., Wu, B., Gao, J., Yang, Z., Zhang, C., 2020. Provenance and transport process for interdune sands in the kumtagh sand sea, northwest China. Geomorphology 367, 107310. https://doi.org/10.1016/j.geomorph.2020.107310.
Liu, J., He, W., Cao, L., Zhu, Z., Xiang, R., Li, T., Shi, X., Liu, S., 2019. Staged fine-grained sediment supply from the Himalayas to the Bengal Fan in response to climate change over the past 50,000 years. Quat. Sci. Rev. 212, 164–177.
Maddison, A., 2001. The World Economy: A Millennial Perspective. OECD, DevelopmentCentre of the Organization for Economic Cooperation and Development, Paris, p. 383p.
Mann, M.E., Jones, P.D., 2003. Global surface temperatures over the past two millenia. Geophys. Res. Lett. 30 (15), 5-1.
McClish, M., Olivelle, P., 2012. The Arthasastra: Selections from the Classic Indian Work on Statecraft. Hackett Publishing, p. 170.
McIntosh, J., 2007. The Ancient Indus Valley: New Perspectives. ABC-CLIO, Santa Barbara, p. 440p.
Mishra, V., Tiwari, A.D., Aadhar, S., Shah, R., Xiao, M., Pai, D.S., Lettenmaier, D., 2019. Drought and famine in India, 1870–2016. Geophys. Res. Lett. 46 (4), 2075–2083.
Moy, C.M., Seltzer, G.O., Rodbell, D.T., Anderson, D.M., 2002. Variability of El niño/southern oscillation activity at millennial timescales during the Holocene epoch. Nature 420 (6912), 162–165.
Naithani, B.D., 1984. Flora of Chamoli-, vols. 1 and 2. Botanical survey of India, Dehradun, p. 789p.
Neukom, R., Steiger, N., Gómez-Navarro, J.J., Wang, J., Werner, J.P., 2019. No evidence for globally coherent warm and cold periods over the preindustrial Common Era. Nature 571, 550–554.
Oldfield, F., Wake, R., Boyle, J., Jones, R., Nolan, S., Gibbs, Z., Appleby, P., Fisher, E., Wolff, G., 2003. The late-Holocene history of Gormire Lake (NE England) and its catchment: a multiproxy reconstruction of past human impact. Holocene 13 (5), 677–690.
Pandey, D.N., Gupta, A.K., Anderson, D.M., 2003. Rainwater harvesting as an adaptation to climate change. Curr. Sci. 85 (1), 46–59.
Paterson, G.A., Heslop, D., 2015. New methods for unmixing sediment grain size data. G-cubed 16 (12), 4494–4506.
Peters, C., Dekkers, M.J., 2003. Selected room temperature magnetic parameters as a function of mineralogy, concentration and grain size. Phys. Chem. Earth A/B/C 28 (16), 659–667.
Phadtare, N.R., 2000. Sharp decrease in summer monsoon strength 4000–3500 cal yr BP in the Central Higher Himalaya of India based on pollen evidence from alpine peat. Quat. Res. 53 (1), 122–129.
Possehl, G.L., 2002. The Indus Civilization: a Contemporary Perspective. Rowman Altamira, p. 275p.
Prasad, S., Anoop, A., Riedel, N., Sarkar, S., Menzel, P., Basavaiah, N., Krishnan, R., Fuller, D., Plessen, B., Gaye, B., Röhl, U., 2014. Prolonged monsoon droughts and links to Indo-Pacific warm pool: a Holocene record from Lonar Lake, central India. Earth Planet Sci. Lett. 391, 171–182.
Rawat, S., Gupta, A.K., Sangode, S.J., Srivastava, P., Nainwal, H.C., 2015a. Late Pleistocene–Holocene vegetation and Indian summer monsoon record from the Lahaul, northwest Himalaya, India. Quat. Sci. Rev. 114, 167–181.
Rawat, S., Gupta, A.K., Srivastava, P., Sangode, S.J., Nainwal, H.C., 2015b. A 13,000 year record of environmental magnetic variations in the lake and peat deposits

from the Chandra valley, Lahaul: implications to Holocene monsoonal variability in the NW Himalaya. Palaeogeogr. Palaeoclimatol. Palaeoecol. 440, 116–127.
Rawat, V., Rawat, S., Srivastava, P., Negi, P.S., Prakasam, M., Kotlia, B.S., 2021. Bednikund lake dataset. Mendeley Data V1. https://doi.org/10.17632/zkn8rs76hy.1.
Reimer, P.J., Bard, E., Bayliss, A., Beck, J.W., Blackwell, P.G., Ramsey, C.B., Buck, C.E., Cheng, H., Edwards, R.L., Friedrich, M., Grootes, P.M., 2013. IntCal13 and Marine13 radiocarbon age calibration curves 0–50,000 years cal BP. Radiocarbon 55 (4), 1869–1887.
Rein, B., Lückge, A., Reinhardt, L., Sirocko, F., Wolf, A., Dullo, W.C., 2005. El Niño variability off Peru during the last 20,000 years. Paleoceanography 20, PA4003. https://doi.org/10.1029/2004PA001099.
Richards, J.F., 1995. The Mughal Empire. Cambridge University Press, ISBN 978-0-521-56603-2.
Schmidt, K.J., 2015. An Atlas and Survey of South Asian History. Routledge, ISBN 978-1-317-47681-8, p. 167.
Sharmila, S., Joseph, S., Sahai, A.K., Abhilash, S., Chattopadhyay, R., 2015. Future projection of Indian summer monsoon variability under climate change scenario: an assessment from CMIP5 climate models. Global Planet. Change 124, 62–78.
Siddiqui, I.H., 1986. Water works and irrigation system in India during pre-Mughal times. J. Econ. Soc. Hist. Orient 29 (1), 52–77.
Sinha, A., Cannariato, K.G., Stott, L.D., Cheng, H., Edwards, R.L., Yadava, M.G., Ramesh, R., Singh, I.B., 2007. A 900-year (600 to 1500 AD) record of the Indian summer monsoon precipitation from the core monsoon zone of India. Geophys. Res. Lett. 34 (16).
Sinha, A., Kathayat, G., Weiss, H., Li, H., Cheng, H., Reuter, J., Schneider, A.W., Berkelhammer, M., Adalı, S.F., Stott, L.D., Edwards, R.L., 2019. Role of climate in the rise and fall of the Neo-Assyrian Empire. Science Advances 5 (11), eaax6656.
Snowball, I.F., 1993. Geochemical control of magnetite dissolution in subarctic lake sediments and the implications for environmental magnetism. J. Quat. Sci. 8 (4), 339–346.
Srivastava, P., Jovane, L., 2020. Misinterpreting proxy data for paleoclimate signals: a comment on Shukla et al. Holocene 30, 1866–1873. https://doi.org/10.1177/0959683620941165, 2020.
Srivastava, R.N., Ahmad, A., 1979. Geology and structure of Alaknanda valley, garhwal Himalaya. Himal. Geol. 9, 225–254.
Staubwasser, M., Sirocko, F., Grootes, P.M., Segl, M., 2003. Climate change at the 4.2 ka BP termination of the Indus valley civilization and Holocene south Asian monsoon variability. Geophys. Res. Lett. 30 (8).
Stein, B., 2010. A History of India, vol. 9. John Wiley & Sons.
Steinhilber, F., Beer, J., Fröhlich, C., 2009. Total solar irradiance during the Holocene. Geophys. Res. Lett. 36, L19704. https://doi.org/10.1029/2009GL040142.
Stewart, G.R., Turnbull, M.H., Schmidt, S., Erskine, P.D., 1995. ^{13}C natural abundance in plant communities along a rainfall gradient: a biological integrator of water availability. Funct. Plant Biol. 22 (1), 51–55.
Stockhausen, H., Thouveny, N., 1999. Rock-magnetic properties of Eemian maar lake sediments from Massif Central, France: a climatic signature? Earth Planet Sci. Lett. 173 (3), 299–313.
Talbot, M.R., Livingstone, D.A., 1989. Hydrogen index and carbon isotopes of lacustrine organic matter as lake level indicators. Palaeogeogr. Palaeoclimatol. Palaeoecol. 70 (1–3), 121–137.
Tamuntuan, G., Bijaksana, S., King, J., Russell, J., Fauzi, U., Maryunani, K., Aufa, N., 2015. Variation of magnetic properties in sediments from Lake Towuti, Indonesia, and its paleoclimatic significance. Palaeogeogr. Palaeoclimatol. Palaeoecol. 420, 163–172.
Thapar, R., 1990. A History of India (Penguin UK).
Trautmann, T.R., 2011. India: Brief History of a Civilization. Oxford University Press, p. 238p.
Uberoi, C., 2012. Little Ice age in mughal India: solar minima linked to droughts? Eos, Transactions American Geophysical Union 93 (44), 437–438.
Valdiya, K.S., 1980. Geology of the Kumaun Lesser Himalaya. Wadia Institute of Himalayan Geology, Dehradun, p. 291p.
Wang, H., Song, Y., Cheng, Y., Luo, Y., Gao, Y., Deng, L., Liu, H., 2016. Mineral magnetism and other characteristics of sediments from a sub-alpine lake (3080 m asl) in central east China and their implications on environmental changes for the last 5770 years. Earth Planet Sci. Lett. 452, 44–59.
Wang, J., Zhu, L., Nishimura, M., Nakamura, T., Ju, J., Xie, M., Takahiro, W., Testsuya, M., 2009. Spatial variability and correlation of environmental proxies during the past 18,000 years among multiple cores from Lake Pumoyum Co, Tibet, China. J. Paleolimnol. 42, 303–315.
Wang, Y., Cheng, H., Edwards, R.L., He, Y., Kong, X., An, Z., Wu, J., Kelly, M.J., Dykoski, C.A., Li, X., 2005. The Holocene Asian monsoon: links to solar changes and North Atlantic climate. Science 308 (5723), 854–857.
Weiss, H., Bradley, R.S., 2001. What drives societal collapse? Science 291 (5504), 609–610.
Williamson, D., Jelinowska, A., Kissel, C., Tucholka, P., Gibert, E., Gasse, F., Massault, M., Taieb, M., Van Campo, E., Wieckowski, K., 1998. Mineral-magnetic proxies of erosion/oxidation cycles in tropical maar-lake sediments (Lake Tritrivakely, Madagascar): paleoenvironmental implications. Earth Planet Sci. Lett. 155 (3–4), 205–219.
Witzel, M., 1987. In: Eggermont Jubilee Volume, P.H.L., Pollet, G. (Eds.), India and the Ancient World. History, Trade and Culture before A.D. 650, vol. 25. Orientalia Lovaniensia Analecta Leuven, pp. 173–213.
Witzel, M., 1995. Early sanskritization. Origins and development of the kuru state. Electron. J. Vedic Stud. 1 (4), 1–26.
Wright, R.P., 2010. The Ancient Indus: Urbanism, Economy, and Society. Cambridge University Press, Cambridge, p. 416p.
Yadava, A.K., Braeuning, A., Singh, J., Yadav, R.R., 2016. Boreal spring precipitation variability in the cold arid western Himalaya during the last millennium, regional linkages, and socio-economic implications. Quat. Sci. Rev. 144, 28–43.
Yanhong, W., Lücke, A., Zhangdong, J., Sumin, W., Schleser, G.H., Battarbee, R.W., Weilan, X., 2006. Holocene climate development on the central Tibetan Plateau: a sedimentary record from Cuoe Lake. Palaeogeogr. Palaeoclimatol. Palaeoecol. 234 (2–4), 328–340.
Yu, X., Li, T., Gu, D., Feng, A., Liu, S., Li, P., Xu, G., Yan, W., Zhang, Z., Zhu, Z., 2019. Sediment transport in the Luanhe River delta: grain size trend analysis. Journal of Oceanology and Limnology 37 (3), 982–997.